

Cyclotron motion in the vicinity of a Lifshitz transition in graphite

M. Orlita,^{1,2} P. Neugebauer,¹ C. Faugeras,¹ A.-L. Barra,¹ M. Potemski,¹ F. M. D. Pellegrino,^{3,4} and D. M. Basko⁵

¹Laboratoire National des Champs Magnétiques Intenses, CNRS-UJF-UPS-INSA, Grenoble, France

²Charles University, Faculty of Mathematics and Physics, Ke Karlovu 5, 121 16 Praha 2, Czech Republic

³Dipartimento di Fisica e Astronomia, Università di Catania, Via S. Sofia 64, I-95123 Catania, Italy

⁴CNISM, UdR Catania, I-95123 Catania, Italy

⁵Université Grenoble 1/CNRS, LPMMC UMR 5493, B.P. 166, 38042 Grenoble, France

Graphite, a model (semi)metal with trigonally warped bands, is investigated with magneto-absorption experiment and viewed as an electronic system in the vicinity of the Lifshitz transition. A characteristic pattern of up to twenty cyclotron resonance harmonics has been observed. This large number of resonances, their relative strengths and characteristic shapes trace the universal properties of the electronic states near a separatrix in the momentum space. Quantum-mechanical perturbative methods with respect to the trigonal warping term hardly describe the data which are, on the other hand, fairly well reproduced within a quasi-classical approach and conventional band structure model. Trigonal symmetry is preserved in graphite in contrast to a similar system, bilayer graphene.

Lifshitz transition [1] (also known as electronic topological transition) is a change in the Fermi surface topology occurring upon a continuous change of some external parameter, such as pressure [2], magnetic field [3] or, most naturally, doping [4]. This transition does not involve a symmetry breaking, alike conventional phase transitions of the Landau type, but still leads to observable singularities in thermodynamics, electron transport, sound propagation, and magnetic response of metals [5]. Saddle points in electronic dispersion, often apparent in complex metals, have only recently been visualized with the spectroscopy method of angle-resolved photoemission [6]. In this Letter, we show how the proximity to a Lifshitz transition manifests itself in cyclotron resonance (CR) absorption experiments on graphite, a model system with saddle points due to the trigonal warping of electronic bands [7].

Classically, CR can be understood from the equation of motion for an electron in a magnetic field \mathbf{B} [1]:

$$d\mathbf{p}/dt = (e/c) [\mathbf{v} \times \mathbf{B}], \quad (1)$$

where $\mathbf{p} = \hbar\mathbf{k}$ is the electron quasi-momentum, $e = -|e|$ the electron charge, and $\mathbf{v} = \partial\epsilon(\mathbf{p})/\partial\mathbf{p}$ is the electron velocity, determined by the dispersion $\epsilon(\mathbf{p})$. Since both the energy ϵ and the momentum component p_z along \mathbf{B} are conserved, the motion occurs along cyclotron orbits in the (p_x, p_y) plane, determined by the condition $\epsilon(p_x, p_y, p_z) = \text{const}$. This motion is periodic, and its period, $2\pi/\omega_c$, being proportional to the cyclotron mass, defines the cyclotron frequency $\omega_c = \omega_c(\epsilon, p_z)$. When an electric field, oscillating at frequency ω , is applied, the electron can absorb energy. Absorption becomes resonant when the perturbation frequency ω matches the cyclotron frequency ω_c or its integer multiple.

In good metals, the incoming radiation is efficiently screened and penetrates the sample only within a thin skin layer. CR absorption is then a surface effect, observed mainly when the magnetic field is parallel to the

surface [9, 10]. This makes CR for good metals a less efficient tool for probing the Fermi surface, as compared to other methods, such as, e. g., de Haas–van Alphen effect. The resonant absorption is also often smeared by the dependence of ω_c on p_z , which is an additional disadvantage.

We have applied the CR absorption technique to study the cyclotron motion in the vicinity of the Lifshitz transition in graphite. The low-temperature in-plane conductivity of this material is relatively low, $\sigma \sim 10^7 - 10^8 (\Omega \cdot \text{m})^{-1}$, and it quickly decreases upon the application of a magnetic field [7, 11]. The skin depth thus reaches tens of nanometers and greatly exceeds the spacing between adjacent graphene layers. Moreover, graphite is a highly anisotropic crystal with rather flat electronic dispersion in the z direction (perpendicular to the layers). It appears as a suitable material for CR studies of the electronic system near the Lifshitz transition driven by the trigonal warping of electronic bands.

CR absorption was measured using the setup routinely applied to high-frequency electron paramagnetic resonance experiments [12]. A flake of natural graphite (50 μm thick, area 1 mm^2) was placed in a Fabry-Perot cavity mounted inside a superconducting coil. The magnetic field was applied perpendicular to the graphene layers. Linearly polarized microwave radiation from a Gunn diode tripled to frequency of 283.2 GHz (1.171 meV) was delivered to the sample via quasi-optics waveguides. The field-modulation technique was applied to enhance the detection sensitivity. The modulation amplitude was chosen in a way to maximize the signal but to not distort the measured lineshapes.

A representative experimental spectrum (raw data) is shown in Fig. 1(a). This trace represents the response of the natural graphite specimen measured as a function of the magnetic field at fixed microwave frequency. Because of the field modulation technique, it corresponds to the derivative of the absorbed power with respect to B . The

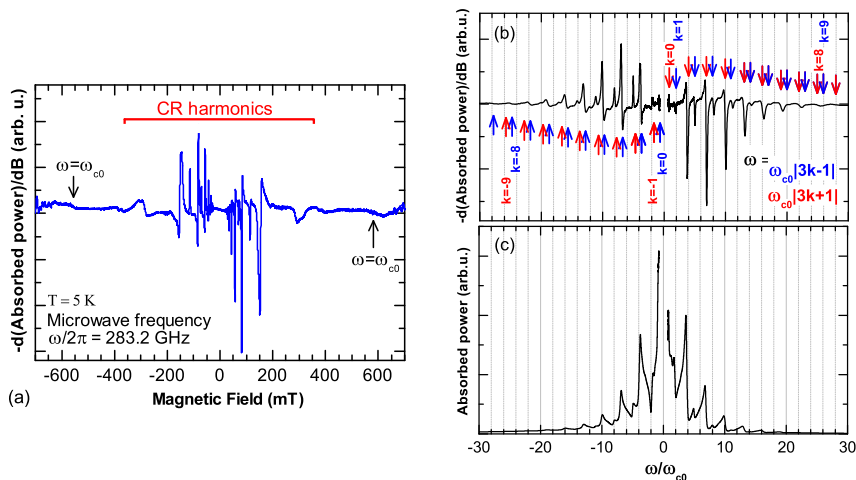


FIG. 1. (color online) Magneto-absorption spectra of natural graphite measured at a fixed microwave excitation energy $\hbar\omega = 1.171$ meV and detected with the help of the field modulation technique at temperature of 5 K. Harmonics of fundamental CR frequency $\omega_{c0} = eB/m_{c0}$ ($m_{c0} = 0.057m_0$) are observed down to fields of 20 mT. (a) Derivative of the absorption with respect to the magnetic field B , as a function of B . (b) The same plotted as a function of ω/ω_{c0} , so that individual harmonics at frequencies of $|3k \pm 1|\omega_{c0}$, $k = 0, \pm 1, \pm 2, \dots$, are clearly seen, as marked by vertical arrows. (c) Absorption as a function of ω/ω_{c0} obtained by the numerical integration of the curve presented in part (a) with respect to B .

magneto-absorption response of graphite is expected to be mostly sensitive to singularities in the electronic joint density of states, located at the K and H points of the graphite Brillouin zone. A number of the observed resonances can be easily identified as due to electronic states at the K point, along the results of previous similar studies [13–18]. Holes at the H point as well as decoupled sheets of graphene on the surface of graphite give rise to resonances at different spectral range (much lower magnetic fields) [19, 20].

To a very first approximation, the K point electrons of graphite have parabolic dispersion. Their effective mass, most frequently reported to be in the range from $m = 0.057m_0$ to $0.060m_0$ [7] (m_0 free electron mass), fixes the cyclotron frequency at $\hbar\omega_{c0} \approx 2 \times B[\text{T}]$ meV. Then, the broad but still visible resonance at $|B| \approx 0.6$ T is attributed to the fundamental CR absorption. All other observed resonances are higher harmonics of the fundamental one. This is evidenced in Fig. 1(b) where the spectrum from Fig. 1(a) is re-plotted against ω/ω_{c0} (i.e. versus B^{-1} instead of B). $\hbar\omega_{c0}$ is eventually set at $2.05 \times B[\text{T}]$ meV. In agreement with previous reports [13], the observed harmonics follow two series: $\omega \approx |3k \pm 1|\omega_{c0}$, where $k = 0, \pm 1, \pm 2, \dots$

The superior quality of the present data (due to higher frequencies applied and perhaps better quality of graphite specimens) allows us to uncover more and intriguing spectral features. Our key observations, that we interpret in the following, are: i) the appearance of a large number (up to 20) of CR harmonics ii) an enhanced strength of $3k + 1$ harmonics as compared to the strength of the $3k - 1$ series at $B > 0$ (and *vice versa* at $B < 0$) and finally, iii) a very characteristic, asymmetric broadening of the observed resonances, enhanced on the low frequency (high-field) sides of the absorption peaks. These features are clearly seen in the raw data and also in Fig. 1(c) in which we reproduce the actual absorption

spectrum, as derived from the numerical integration, over the magnetic field, of the measured (differential) signal.

The appearance of n -harmonics with $n = 3k \pm 1$ is usually understood as due to breaking of the isotropy of the electronic spectrum in the layer plane by the trigonal warping. For isotropic bands, only the $k = 0$ fundamental transition is allowed, whereas the $n = 3k \pm 1$ harmonic appears in the $|k|$ th order of the perturbation theory with respect to the trigonal warping term [16, 21]. The spectrum in Fig. 1 contains many harmonics which start to fall off only at large indices $n \gtrsim 7$. Clearly, the perturbation theory is not applicable to interpret these data. Instead, we will use the quasi-classical approximation.

Eq. (1) can be cast in the Hamiltonian form in the phase space (p_x, p_y) : $dp_x/dt = -\partial\mathcal{H}(p_x, p_y)/\partial p_y$, $dp_y/dt = \partial\mathcal{H}(p_x, p_y)/\partial p_x$, with the Hamiltonian $\mathcal{H}(p_x, p_y) = -(eB/c)\epsilon(p_x, p_y)$ (we omitted p_z , which enters as a parameter). Generally, classical Hamiltonian systems exhibit a very rich behavior. However, they share some universal features when the energy ϵ is close to that of a saddle point of the Hamiltonian, $\epsilon = \epsilon_{sp}$, as is well-known in the classical nonlinear physics [22]. (i) The cyclotron motion in the vicinity of a saddle point is slow and its period diverges logarithmically, $\omega_c(\epsilon) \rightarrow 0$ for $\epsilon \rightarrow \epsilon_{sp}$. (ii) The Fourier spectrum of this motion contains many harmonics and their number diverges when $\epsilon \rightarrow \epsilon_{sp}$. This second fact provides an obvious hint for the interpretation of the experimental data.

The experimentally probed electronic states are those around the Fermi level ϵ_F . Thus, the effects discussed above are important if $\epsilon_F \approx \epsilon_{sp}$. This is the case of graphite, as illustrated in Fig. 2 using standard calculations based on the Slonczewski-Weiss-McClure (SWM) model [23] in the two-band approximation (see Supplementary Information). Here we used the standard values of the SWM parameters [7]: $\gamma_0 = 3150$ meV, $\gamma_1 = 375$ meV, $\gamma_2 = -20$ meV, $\gamma_3 = 315$ meV, $\gamma_4 = 44$ meV,

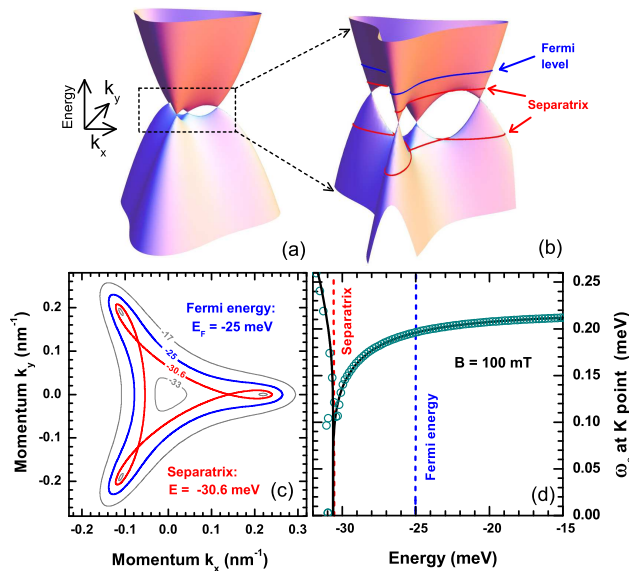


FIG. 2. (color online) (a,b) Electronic structure near the K point of graphite ($k_z = 0$). Two separatrix lines pass through six saddle points. The Fermi level is located about 6 meV above the upper separatrix. (c) Constant energy contours in the (k_x, k_y) plane for $k_z = 0$ for $\epsilon = -17$, $\epsilon = -25$ (Fermi level), $\epsilon = -30.6$ (upper separatrix), and $\epsilon = -33$ meV. (d) Classical cyclotron frequency $\hbar\omega_c(\epsilon, k_z = 0)$ at $B = 100$ mT in the relevant energy interval. ω_c vanishes at the saddle point. Open circles show the LL spacing, $\Delta\epsilon_l = \epsilon_{l+1} - \epsilon_l$, as a function of ϵ_l , derived from the SWM model. Roughly 1 meV away from the saddle point, the circles fall on the classical curve, $\Delta\epsilon_l \approx \hbar\omega_c(\epsilon_l)$.

$\gamma_5 = 38$ meV, $\Delta = -8$ meV. The band dispersion has six saddle points at two different energies ϵ_{e-sp} and ϵ_{h-sp} , which define two separatrices – isoenergetic lines separating regions with different topology. Fermi level crossing these saddle points would imply the change in the topology of the Fermi surface, which actually corresponds to the Lifshitz transition of the neck-collapsing type. The Fermi level is close to the upper separatrix, on which we focus our attention hereafter, $\epsilon_{sp} \equiv \epsilon_{e-sp}$. The single electron pocket around the K point at $\epsilon_F > \epsilon_{sp}$, splits into four disconnected pockets when ϵ_F goes below ϵ_{sp} . Fig. 2(d) shows the classical cyclotron frequency for the SWM dispersion at $k_z = 0$, which vanishes at $\epsilon = \epsilon_{sp}$.

In the language of quantum mechanics, the $k_z = 0$ energy spectrum consists of discrete Landau levels (LLs) ϵ_l . In the quasiclassical approximation, ϵ_l can be found from the Bohr-Sommerfeld quantization rule. The n^{th} CR harmonic corresponds to the transition over n levels, $n\hbar\omega_c \approx \epsilon_{l+n} - \epsilon_l$, to the leading order in \hbar . The decrease of $\omega_c(\epsilon)$ at $\epsilon \rightarrow \epsilon_{sp}$ corresponds to an accumulation of LLs. Nevertheless, $\Delta\epsilon$ does not approach zero, since the condition of the validity of the quasiclassical quantization, $|\omega_c(\epsilon + \hbar\omega_c) - \omega_c(\epsilon)| \ll \omega_c(\epsilon)$, holds only if ϵ is not too close to ϵ_{sp} . LLs always remain discrete, see Fig. 2(d).

As we will show later, $\epsilon_F - \epsilon_{sp}$ is about 6 meV, i.e., it is five times larger than the microwave frequency, $\hbar\omega = 1.171$ meV. Our classical approximation is justified in this case. As a matter of fact, the quasi-classical approximation works the better, the smaller ω is. However, if microwave frequency is too small, the harmonic structure will be smeared by broadening of electronic states. The optimal frequency, used in the experiment, is thus determined by an appropriate compromise between these two competing conditions.

Assuming that the absorbed power is proportional to the real part of the conductivity, $\text{Re}\sigma_{xx}(\omega)$, and calculating the latter from the standard kinetic equation [1] in the simplest relaxation time approximation for the collision integral (see Supplementary Information), we obtain

$$\text{Re}\sigma_{xx}(\omega) = \frac{e^2}{\pi^2\hbar} \sum_{n=-\infty}^{\infty} \int \left(-\frac{\partial f}{\partial \epsilon} \right) \frac{\Gamma m_c |v_{x,n}|^2 dk_z d\epsilon}{\hbar^2(\omega - n\omega_c)^2 + \Gamma^2}, \quad (2)$$

where the k_z integration is from $-\pi/(2a_z)$ to $\pi/(2a_z)$. Both the cyclotron frequency, ω_c , and the cyclotron mass, $m_c = -eB/(c\omega_c)$, depend on ϵ and k_z . The basic frequency ω_{c0} , introduced earlier, is $\omega_{c0} = \omega_c(\epsilon = \epsilon_F, k_z = 0)$. $\mathbf{v}_n = \mathbf{v}_n(\epsilon, k_z)$ is the Fourier harmonic of the electron velocity, corresponding to the term $\propto e^{-in\omega_c t}$, determined from the solution of the unperturbed equation of motion, Eq. (1). Finally, Γ accounts for relaxation, and $f(\epsilon)$ is the Fermi function.

Even without solving Eq. (1), it is easy to see that the triangular symmetry of $\epsilon(\mathbf{p})$ in the (p_x, p_y) plane fixes $\mathbf{v}_n = 0$ for $n = 3k$, $k = \pm 1, \pm 2, \dots$. In Fig. 1(b), the resonances at $n = 3k$ are absent, which demonstrates that the triangular symmetry is not broken in graphite. This is in contrast with recent reports for a bilayer graphene [24–27], even though it is formally described by the same single-particle Hamiltonian (for a fixed k_z) [28]. The same symmetry fixes $v_{n,x}$ to be real and $v_{n,y} = \pm i v_{n,x}$ for $n = 3k \pm 1$, so the peaks at $n = 3k + 1$ and $n = 3k - 1$ are seen in the opposite circular polarizations of the microwave field. This helps us to understand the observed difference in the intensities of the $n = 3k + 1$ and $n = 3k - 1$ series. Indeed, for $B > 0$, when the electron moves along the Fermi surface, shown in Fig. 2(b), in the overall counterclockwise direction, it should be more strongly coupled to the counterclockwise polarized radiation. As both circular polarizations are equally present in the incoming linearly polarized radiation, the spectrum is fairly symmetric with respect to $B \rightarrow -B$.

The present studies are restricted to bulk graphite, a system with fixed Fermi level but in an apparent proximity to the Lifshitz transition. An obvious experimental challenge would be to trace the CR response when changing the Fermi level with respect to the separatrix energy, with an attempt to tune the proximity to Lifshitz transition in graphitic structures. This can be

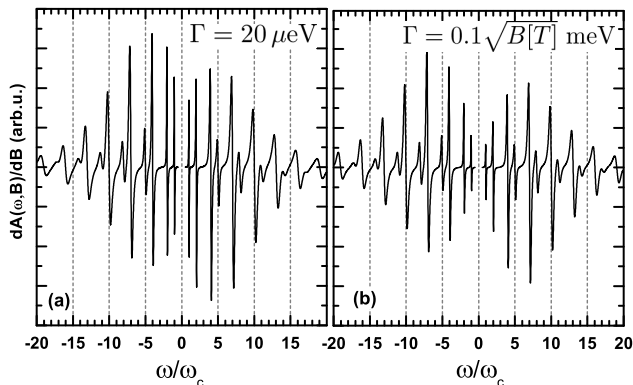


FIG. 3. Derivative of the absorption with respect to B , as calculated using Eq. (2) for different electronic broadenings Γ . (a) a constant broadening $\Gamma = 20 \mu\text{eV}$ and (b) $\Gamma = 0.1\sqrt{B[\text{T}]}$ meV.

in principle envisaged for electrostatically gated bilayer graphene [26, 27] and/or for bulk graphite under hydrostatic pressure [29]. Importantly, such experiments require no degradation of the quality of the sample, which likely excludes the experiments on, for example, chemically doped structures.

Besides the large number of harmonics, typical of a classical motion near a saddle point, the proximity to the Lifshitz transition also leads to some lowering of the cyclotron frequency. Indeed, the fundamental cyclotron frequency determined from the period in B^{-1} of the spectrum, $\hbar\omega_{c0}/B = 2.05 \text{ meV/T}$, is slightly lower than its parabolic-band limit at $k_z = 0$, 2.24 meV/T . The latter value, however, relies on the specific values of the parameters of the SWM model. More apparent effects are deduced from the analysis of the peak shapes (which are determined by the integration over k_z).

As seen from Fig. 1(c), each peak has an abrupt cut-off on the *high-frequency* side and a tail on the *low-frequency* side. This contradicts the first intuition, based on the well-known fact that the parabolic part of the bands becomes steeper as k_z increases from the K point towards the H point. This pushes the LLs upwards as k_z increases and would result in a tail on the *high-frequency* side of each peak in the absorption spectrum $\mathcal{A}(\omega, B)$ [30]. However, the bottom of the conduction band [defined as $\epsilon(\mathbf{p} = 0, k_z)$] and the saddle point $\epsilon_{\text{sp}}(k_z)$ shift upwards upon increasing k_z , as $\epsilon(\mathbf{p} = 0, k_z) = 2\gamma_2 \cos k_z a_z$, $\gamma_2 < 0$. Thus, the Fermi level approaches the saddle point as k_z moves away from $k_z = 0$ point and $\omega_c(\epsilon_F, k_z)$ decreases simultaneously, see Fig. 2(d). This provides a tail on the *low-frequency* side of the peaks. Thus, the suppression of ω_c near the Lifshitz transition is crucial to interpret the peak asymmetry.

The spectrum derived from Eq. (2) is shown in Fig. 3, with ϵ_F and Γ as the only adjustable parameters – the parameters of the SWM model were fixed [7]. The

best agreement is obtained for $\epsilon_F = -25 \text{ meV}$. If $\epsilon_F = -24 \text{ meV}$, the peaks have no asymmetry, since $\omega_c(\epsilon_F = -24 \text{ meV}, k_z)$ has a significant upturn on increasing k_z . When $\epsilon_F = -26 \text{ meV}$ the fall-off of large- n harmonics is noticeably slower than the experimental one. In other words, the closer ϵ_F is to ϵ_{sp} , the more harmonics are seen in the spectrum. The frequency $\omega_c(\epsilon_F = -25 \text{ meV}, k_z = 0)/B = 2.03 \text{ meV/T}$ agrees with the experimental value, 2.05 meV/T . The value $\epsilon_F = -25 \text{ meV}$ is also in good agreement with the one determined independently from the charge neutrality condition (see Supplementary Information), $\epsilon_F = -24 \text{ meV}$. A constant value of $\Gamma = 20 \mu\text{eV}$ was assumed for the curve in Fig. 3(a). Apparently, this does not describe well the amplitudes of peaks at $n = 1, 2$: the theoretical peaks are narrower and thus more intense than the experimental ones. Better agreement is obtained under assumption that $\Gamma \propto \sqrt{B}$ (see Ref. 3 and Supplementary Information). Notably, the curve in Fig. 3(b) with $\Gamma = 0.1\sqrt{B[\text{T}]}$ meV corresponds to the zero-field relaxation rate $\hbar/\tau_{B=0} = 40 \mu\text{eV}$. The extracted value of $\tau_{B=0}$ provides the zero-field dc conductivity $\sigma = 1.2 \times 10^8 (\Omega \cdot \text{m})^{-1}$ (see Supplementary Information). This is fully consistent with typical literature data [7, 11] and implies a mean electron free path of $6 \mu\text{m}$, which is, notably, comparable or even longer than the corresponding values reported for strictly 2D graphene-based structures [26, 32, 33].

To conclude, we have introduced CR experiments as a new tool to study Lifshitz transitions. We have shown how the proximity to the Lifshitz transition manifests itself in the CR spectrum of a model system, bulk graphite. Namely, we have observed a multi-mode response, where the basic CR mode is accompanied by many harmonics. Using the standard SWM model for the electronic band structure of graphite to analyze the data, we have determined the Fermi energy and estimated the electronic broadening. The similarity between the band structure of graphite near the K point and that of a bilayer graphene logically suggests to probe Lifshitz transition in the latter system by CR methods, and to shed more light on the currently debated issue of spontaneous symmetry breaking in bilayer graphene [24–27].

We thank M.-O. Goerbig and J.-N. Fuchs for collaboration on the early stages of this work, and V. F. Gantmakher and Yu. I. Latyshev for helpful discussions. Part of this work was supported by RTRA “DISPOGRAPH” project. M.O. acknowledges support from GACR P204/10/1020 and GRA/10/E006 (EPIGRAT). F. M. D. P. thanks LPMCM for hospitality.

-
- [1] I. M. Lishitz, Zh. Eksp. Teor. Fiz. **38**, 1565 (1960).
 [2] V. I. Makarov and Bar'yakhtar, Zh. Eksp. Teor. Fiz. **48**, 1717 (1965), and references therein; C. W. Chu, T. F.

- Smith, and W. E. Gardner, Phys. Rev. B **1**, 214 (1970); B. K. Godwal *et al.*, Phys. Rev. B **57**, 773 (1998).
- [3] P. M. C. Rourke *et al.*, Phys. Rev. Lett. **101**, 237205 (2008); J. Wosnitza *et al.*, Physica B **403**, 1219 (2008).
- [4] D. Yoshizumi *et al.*, J. Phys. Soc. Japan **76**, 063705 (2007); Y. Okamoto, A. Nishio, A., and Z. Hiroi, Phys. Rev. B **81**, 121102(R) (2010); S. E. Sebastian *et al.*, Proc. Nat. Acad. Sci. **107**, 6175 (2010); M. R. Norman, J. Lin, and A. J. Millis, Phys. Rev. B **81**, 180513(R) (2010); D. LeBoeuf, *et al.* Phys. Rev. B **83**, 054506 (2011).
- [5] Y. M. Blanter *et al.*, Phys. Rep. **245**, 159 (1994).
- [6] C. Liu *et al.*, Nature Phys. **6**, 419 (2010).
- [7] N. B. Brandt, S. M. Chudinov, and Y. G. Ponomarev, *Semimetals 1: Graphite and Its Compounds*, (North-Holland, Amsterdam, 1988).
- [8] A. A. Abrikosov, *Fundamentals of the Theory of Metals* (North Holland, Amsterdam, 1988).
- [9] M. Ya. Azbel' and E. A. Kaner, Zh. Eksp. Teor. Fiz. **30**, 811 (1956).
- [10] Khaikin, M. S. *Zh. Eksp. Teor. Fiz.* **41**, 1773–1779 (1961) [*Sov. Phys. JETP* **14**, 1260–1264 (1962)].
- [11] X. Du *et al.*, Phys. Rev. Lett. **94**, 166601 (2005).
- [12] P. Neugebauer and A.-L. Barra, Appl. Magn. Reson. **37**, 833 (2010).
- [13] J. K. Galt, W. A. Yager, and H. W. Dail, Jr., Phys. Rev. **103**, 1586 (1956) S. J. Williamson *et al.*, Solid State Commun. **4**, 37 (1966); H. Suematsu and S. Tanuma, J. Phys. Soc. Jap. **33**, 1619 (1972).
- [14] B. Lax and H. J. Zeiger, Phys. Rev. **105**, 1466 (1957).
- [15] P. Nozières, Phys. Rev. **109**, 1510 (1958).
- [16] M. Inoue, J. Phys. Soc. Jpn. **17**, 808 (1962).
- [17] G. Dresselhaus, Phys. Rev. B **10**, 3602 (1974).
- [18] R. E. Doezma *et al.*, Phys. Rev. B **19**, 4224 (1979).
- [19] M. Orlita *et al.*, Phys. Rev. Lett. **100**, 136403 (2008).
- [20] P. Neugebauer *et al.*, Phys. Rev. Lett. **103**, 136403 (2009).
- [21] D. S. L. Abergel and V. I. Fal'ko, Phys. Rev. B **75**, 155430 (2007); L. A. Falkovsky, Phys. Rev. B **84**, 115414 (2011).
- [22] R. Z. Sagdeev, D. A. Usikov, and G. M. Zaslavsky, *Nonlinear Physics: From the Pendulum to Turbulence and Chaos* (Harwood Academic Publishers, New York, 1988).
- [23] J. W. McClure, Phys. Rev. **108**, 612 (1957); J. C. Slonczewski and P. R. Weiss, *ibid* **109**, 272 (1958).
- [24] O. Vafeek and K. Yang, Phys. Rev. B **81**, 041401 (2010)
- [25] Y. Lemonik *et al.*, Phys. Rev. B **82**, 201408(R) (2010).
- [26] A. S. Mayorov *et al.*, Science **333**, 862 (2011).
- [27] M. Mucha-Kruczyński, I. L. Aleiner, and V. I. Fal'ko, Phys. Rev. B **84**, 041404 (2011).
- [28] M. Orlita *et al.*, Phys. Rev. Lett. **102**, 166401 (2009).
- [29] E. Mendez, A. Misu, and M. S. Dresselhaus, Phys. Rev. B **21**, 827 (1980).
- [30] P. Kossacki *et al.*, arXiv:1110.4262.
- [31] T. Ando, J. Phys. Soc. Japan **38**, 989 (1975).
- [32] K. I. Bolotin *et al.*, Phys. Rev. Lett. **101**, 096802 (2008).
- [33] S. A. Mayorov *et al.*, Nano Lett. **11**, 2396 (2011).

Supplementary Information for

Cyclotron motion in the vicinity of Lifshitz transition in graphite

by M. Orlita, P. Neugebauer, C. Faugeras, A.-L. Barra, M. Potemski, F. M. D. Pellegrino, and D. M. Basko

SLONCZEWSKI-WEISS-MCCLURE MODEL AND ITS TWO-BAND PROJECTION

The Hamiltonian of the *AB*-stacked graphite can be written as

$$H = \begin{pmatrix} \dots & \dots \\ \dots & V_{11} & V_{12}^\dagger & H_1 & V_{12}^\dagger & V_{11}^\dagger & 0 & 0 & 0 & \dots \\ \dots & 0 & V_{22} & V_{12} & H_2 & V_{12} & V_{22}^\dagger & 0 & 0 & \dots \\ \dots & 0 & 0 & V_{11} & V_{12}^\dagger & H_1 & V_{12}^\dagger & V_{11}^\dagger & 0 & \dots \\ \dots & 0 & 0 & 0 & V_{22} & V_{12} & H_2 & V_{12} & V_{22}^\dagger & \dots \\ \dots & \dots \end{pmatrix}, \quad (3)$$

where each element is a matrix in the Hilbert space of a single layer. H_1 and H_2 contain the in-plane nearest-neighbor coupling with the matrix element γ_0 as well as the diagonal shift Δ . V_{12} represents the coupling between neighboring layers with matrix elements γ_1 for the neighboring atoms, and γ_3, γ_4 for the second nearest neighbors. V_{11} and V_{22} correspond to second-nearest-layer coupling with matrix elements $\gamma_2/2$ and $\gamma_5/2$. Due to the translational invariance in the z direction, the problem can be reduced to that of an effective bilayer:

$$H_{k_z} = \begin{bmatrix} H_1 + V_{11}e^{2ik_z a_z} + V_{11}^\dagger e^{-2ik_z a_z} & 2V_{12}^\dagger \cos k_z a_z \\ 2V_{12} \cos k_z a_z & H_2 + V_{22}e^{2ik_z a_z} + V_{22}^\dagger e^{-2ik_z a_z} \end{bmatrix}, \quad (4)$$

where a_z is the distance between the neighboring layers, and k_z is the wave vector in the direction perpendicular

to the layers, $-\pi/(2a_z) < k_z \leq \pi/(2a_z)$ (note that

the period of the structure is $2a_z$, that is, two layers). Expansion of the single-layer Hamiltonian in p_x, p_y , the in-plane quasi-momentum components counted from the $H - K - H$ line, gives

$$H_{k_z}(\hat{\mathbf{p}}) = \begin{bmatrix} \Gamma_2 & v\hat{p}_- & -\alpha_4 v\hat{p}_- & \alpha_3 v\hat{p}_+ \\ v\hat{p}_+ & \Gamma_5 & \Gamma_1 & -\alpha_4 v\hat{p}_- \\ -\alpha_4 v\hat{p}_+ & \Gamma_1 & \Gamma_5 & v\hat{p}_- \\ \alpha_3 v\hat{p}_- & -\alpha_4 v\hat{p}_+ & v\hat{p}_+ & \Gamma_2 \end{bmatrix}, \quad (5)$$

where

$$v = \frac{3}{2} \frac{\gamma_0 a}{\hbar}, \quad \Gamma_1 = 2\gamma_1 \mathcal{C}, \quad \Gamma_2 = 2\gamma_2 \mathcal{C}^2, \\ \alpha_{3,4} = \frac{2\gamma_{3,4}}{\gamma_0} \mathcal{C}, \quad \Gamma_5 = 2\gamma_5 \mathcal{C}^2 + \Delta, \quad \mathcal{C} \equiv \cos k_z a_z,$$

$a = 1.42\text{\AA}$ is the distance between the neighboring carbon atoms in the same layer, and $\hat{p}_\pm = -i\hbar(\partial_x \pm i\partial_y)$. It is convenient to rotate the basis in the space of the 4-columns $(\psi_1, \psi_2, \psi_3, \psi_4)^T$ as

$$\psi'_1 = \frac{\psi_2 + \psi_3}{\sqrt{2}}, \quad \psi'_2 = \psi_1, \quad \psi'_3 = \psi_4, \quad \psi'_4 = \frac{\psi_2 - \psi_3}{\sqrt{2}}, \quad (6)$$

so the transformed Hamiltonian becomes

$$H'_{k_z}(\hat{\mathbf{p}}) = \begin{bmatrix} \Gamma_5 + \Gamma_1 & \bar{v}_4 \hat{p}_+ & \bar{v}_4 \hat{p}_- & 0 \\ \bar{v}_4 \hat{p}_- & \Gamma_2 & \alpha_3 v \hat{p}_+ & v_4 \hat{p}_- \\ \bar{v}_4 \hat{p}_+ & \alpha_3 v \hat{p}_- & \Gamma_2 & -v_4 \hat{p}_+ \\ 0 & v_4 \hat{p}_+ & -v_4 \hat{p}_- & \Gamma_5 - \Gamma_1 \end{bmatrix}, \quad (7)$$

where $v_4 = v(1 + \alpha_4)/\sqrt{2}$, $\bar{v}_4 = v(1 - \alpha_4)/\sqrt{2}$. The four eigenvalues for each p_x, p_y, k_z can be found by calculating the determinant

$$\det H'_{k_z}(\mathbf{p}) = (1 - \alpha_4^2)^2 (vp)^4 - \\ - 2\alpha_3 [(1 + \alpha_4^2)\Gamma_1 + 2\alpha_4\Gamma_5] (vp)^3 \cos 3\varphi_{\mathbf{p}} + \\ + [\alpha_3^2(\Gamma_1^2 - \Gamma_5^2) - 2(1 + \alpha_4^2)\Gamma_2\Gamma_5 - 4\alpha_4\Gamma_2\Gamma_1] (vp)^2 - \\ - \Gamma_2^2(\Gamma_1^2 - \Gamma_5^2), \quad (8)$$

and replacing $\Gamma_5 \rightarrow \Gamma_5 - \epsilon$, $\Gamma_2 \rightarrow \Gamma_2 - \epsilon$ to obtain $\det(H'_{k_z} - \epsilon)$.

To obtain the effective 2×2 Hamiltonian, acting in the subspace of the two low-energy bands, we eliminate ψ'_1, ψ'_4 from the Schrödinger equation $H'_{k_z}(\hat{\mathbf{p}})\psi' = \epsilon\psi'$. This gives

$$\hat{H}_{k_z}^{2 \times 2}(\hat{\mathbf{p}}) = \begin{bmatrix} \Gamma_2 & \alpha_3 v \hat{p}_+ - v^2 \hat{p}_-^2 / \Gamma_1 \\ \alpha_3 v \hat{p}_- - v^2 \hat{p}_+^2 / \Gamma_1 & \Gamma_2 \end{bmatrix} - \\ + \frac{2\zeta_{eh}}{\Gamma_1} \begin{bmatrix} v^2 \hat{p}_- \hat{p}_+ & 0 \\ 0 & v^2 \hat{p}_+ \hat{p}_- \end{bmatrix},$$

where

$$\zeta_{eh} = \alpha_4 + \frac{\Gamma_5 - \Gamma_2}{2\Gamma_1} \quad (9)$$

determines the electron-hole asymmetry of the spectrum. At energies we are interested in (a few tens of meV) the two-band approximation works well for all k_z except the immediate vicinity of the H point, $\pi/2 - |k_z|a_z \lesssim 0.05$. In the two-band approximation, there is an analytical expression for the energies, which is most conveniently written in the polar coordinates, $p_x = p \cos \varphi$, $p_y = p \sin \varphi$:

$$\epsilon_{k_z}^\pm(p \cos \varphi, p \sin \varphi) = \Gamma_2 + 2\zeta_{eh} \frac{(vp)^2}{\Gamma_1} \pm \\ \pm \sqrt{\frac{(vp)^4}{\Gamma_1^2} - 2\alpha_3 \frac{(vp)^3}{\Gamma_1} \cos 3\varphi + \alpha_3^2 (vp)^2}. \quad (10)$$

From this expression one can deduce the energies of the saddle point in the conduction band, the energies of the three ‘‘leg’’ conical points, where the conduction and the valence bands touch each other (in addition to the conical point at $\mathbf{p} = 0$ with $\epsilon = \Gamma_2$), and the energy of the saddle point in the valence band:

$$\epsilon_{e\text{-sp}} = \Gamma_2 + \frac{\alpha_3^2 \Gamma_1}{4(1 - 2\zeta_{eh})}, \quad (11a)$$

$$\epsilon_{\text{leg}} = \Gamma_2 + 2\zeta_{eh} \alpha_3^2 \Gamma_1, \quad (11b)$$

$$\epsilon_{h\text{-sp}} = \epsilon_c - \frac{\alpha_3^2 \Gamma_1}{4(1 + 2\zeta_{eh})}. \quad (11c)$$

Given the dispersion (10), one can determine the concentrations of electrons and holes at zero temperature as functions of the Fermi energy,

$$n_e(\epsilon_F) = 4 \int_{\epsilon^+(\mathbf{p}) < \epsilon_F} \frac{d^3 \mathbf{p}}{(2\pi\hbar)^3}, \quad (12a)$$

$$n_h(\epsilon_F) = 4 \int_{\epsilon^-(\mathbf{p}) > \epsilon_F} \frac{d^3 \mathbf{p}}{(2\pi\hbar)^3}, \quad (12b)$$

where the factor of 4 takes care of valley and spin degeneracy. If the sample is undoped, ϵ_F can be determined from the neutrality condition $n_e(\epsilon_F) = n_h(\epsilon_F)$. Electron and hole concentrations obtained from Eqs. (12a), (12b), are plotted in Fig. 4, together with the simplified expression,

$$n_{e,h}(\epsilon_F) = \frac{2\gamma_1 |\epsilon_F| \theta(\pm \epsilon_F)}{\pi^2 a_z (3\gamma_0 a/2)^2} \mathcal{Z}(\pm 4\gamma_4/\gamma_0), \quad (13) \\ \mathcal{Z}(x) \equiv \frac{2}{x} \left(\frac{\pi}{4} - \frac{1}{\sqrt{1-x^2}} \arctan \sqrt{\frac{1-x}{1+x}} \right),$$

obtained by neglecting $\gamma_2, \gamma_3, \gamma_5$.

CONDUCTIVITY FROM THE KINETIC EQUATION

We determine the conductivity from the electronic dispersion following the standard procedure[1]. First, let us

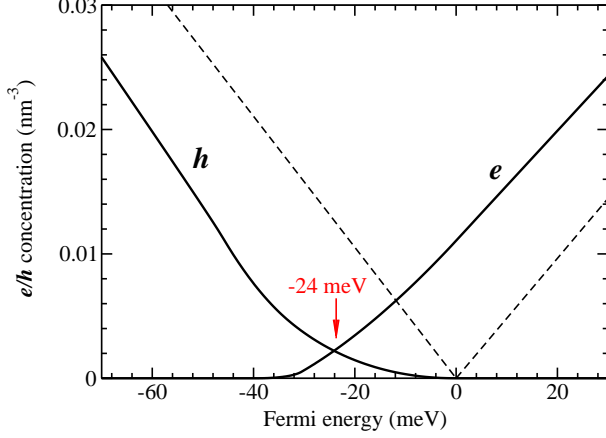


FIG. 4. Electron and hole concentrations as functions of the Fermi energy, as given by Eqs. (12a), (12b) (thick solid lines), together with the simplified expression (13) (dashed lines).

consider the problem at some fixed value of k_z , and find the in-plane electric current produced by an external in-plane electric field

$$\mathbf{E}(t) = \mathbf{E}_\omega e^{-i\omega t} + \mathbf{E}_\omega^* e^{i\omega t}. \quad (14)$$

The in-plane group velocity of the electrons being $\mathbf{v} = \partial\epsilon(\mathbf{p})/\partial\mathbf{p}$ (\mathbf{p} is in the xy plane, and we omit the k_z argument for the moment), the semiclassical equations of motion are

$$\frac{dp_x}{dt} = \frac{eB}{c} \frac{\partial\epsilon(p_x, p_y)}{\partial p_y} + eE_x(t), \quad (15a)$$

$$\frac{dp_y}{dt} = -\frac{eB}{c} \frac{\partial\epsilon(p_x, p_y)}{\partial p_x} + eE_y(t). \quad (15b)$$

Here the electron charge $e < 0$. These equations can be written in the Hamiltonian form $dp_x/dt = -\partial\mathcal{H}/\partial p_y$, $dp_y/dt = \partial\mathcal{H}/\partial p_x$, with the Hamiltonian function

$$\mathcal{H}(p_x, p_y) = -\frac{eB}{c} \epsilon(p_x, p_y) + e(E_y p_x - E_x p_y). \quad (16)$$

In the absence of the perturbing electric field the trajectories in the (p_x, p_y) -space (cyclotron orbits) coincide with the constant energy contours, $\epsilon(\mathbf{p}) = \text{const}$. The solution of the unperturbed problem ($\mathbf{E} = 0$) can be written as

$$\mathbf{p}(t) = \sum_{n=-\infty}^{\infty} \mathbf{p}_n(\epsilon) e^{-in\omega_c(\epsilon)t}, \quad \mathbf{p}_n(\epsilon) = \mathbf{p}_{-n}^*(\epsilon), \quad (17)$$

where the frequency is determined by the derivative of the area, enclosed by the cyclotron orbit, with respect to energy:

$$\omega_c(\epsilon) = -\frac{eB}{m_c(\epsilon)c}, \quad m_c(\epsilon) = \frac{1}{2\pi} \frac{\partial}{\partial\epsilon} \int_{\epsilon(\mathbf{p}) < \epsilon} dp_x dp_y. \quad (18)$$

Thus defined m_c is nothing but the cyclotron mass. The harmonics of the velocity can be related to those of momentum directly from the equations of motion, which gives

$$v_{nx}(\epsilon) = -\frac{in}{m_c(\epsilon)} p_{ny}(\epsilon), \quad v_{ny}(\epsilon) = \frac{in}{m_c(\epsilon)} p_{nx}(\epsilon). \quad (19)$$

The symmetry of the cyclotron orbit with respect to rotations by $2\pi/3$ fixes

$$p_{3k,x} = p_{3k,y} = 0, \quad p_{3k\pm 1,x} = \mp i p_{3k\pm 1,y} = P_{3k\pm 1}, \quad (20)$$

for integer k , where $P_n(\epsilon)$ are real. When $\epsilon_{h-sp} < \epsilon < \epsilon_{e-sp}$, in addition to the orbit which is C_{3v} -symmetric around the origin, for each ϵ there are three other orbits encircling the three ‘‘leg’’ conical points, each such orbit having only one mirror reflection symmetry. These give rise to another series solutions with

$$p_{n,x} = P'_n, \quad p_{n,y} = iQ'_n, \quad (21)$$

where $P'_n(\epsilon)$, $Q'_n(\epsilon)$ are also real. However, we will be mostly concerned with the first solution, Eq. (20).

In order to separate the oscillating motion, it is convenient to perform the canonical change to action-angle variables of the unperturbed Hamiltonian, $(p_x, p_y) \rightarrow (S, \phi)$. The action variable is defined by

$$S(\epsilon) = -\frac{c}{eB} \int_{\epsilon(\mathbf{p}) < \epsilon} \frac{dp_x dp_y}{2\pi}, \quad (22)$$

and the angle $\phi = \omega_c t$ for the unperturbed motion. The inverse transformation, $(S, \phi) \rightarrow (p_x, p_y)$, is given by Eq. (17) with the replacement $\omega_c t \rightarrow \phi$ and $\epsilon \rightarrow \epsilon(S)$, the latter determined from Eq. (22). As for any canonical transformation, the phase volume is preserved: $dp_x dp_y = dS d\phi$. In the new variables, the Hamiltonian (16) assumes the form

$$\mathcal{H}(S, \phi) = \int^S \omega_c(S') dS' + \sum_{n \neq 0} \frac{m_c(S)}{in} e\mathbf{E} \cdot \mathbf{v}_n(S) e^{-in\phi}. \quad (23)$$

The distribution function $\mathcal{F}(S, \phi)$ is defined as the average number of particles in the quantum of the phase volume, $(2\pi\hbar)^2$, around some given values of S, ϕ . It determines the total current carried by the electrons:

$$\mathbf{j}(t) = \int \frac{dS d\phi}{(2\pi\hbar)^2} \mathcal{F}(S, \phi, t) \sum_{n=-\infty}^{\infty} e\mathbf{v}_n(S) e^{-in\phi}. \quad (24)$$

The distribution function \mathcal{F} satisfies the kinetic equation

$$\frac{\partial\mathcal{F}}{\partial t} + \frac{\partial\mathcal{H}}{\partial S} \frac{\partial\mathcal{F}}{\partial\phi} - \frac{\partial\mathcal{H}}{\partial\phi} \frac{\partial\mathcal{F}}{\partial S} = \text{St}[\mathcal{F}], \quad (25)$$

where the left-hand side is the canonical Liouville operator, and the right-hand side represents the collision

integral. We seek the distribution function in the form $\mathcal{F}(S, \phi, t) = \mathcal{F}_0(S) + \delta\mathcal{F}(S, \phi, t)$, where $\mathcal{F}_0(S)$ is the equilibrium distribution function, corresponding to the Fermi-Dirac distribution $f(\epsilon)$:

$$\mathcal{F}_0(S) = f(\epsilon(S)) = \frac{1}{1 + e^{[\epsilon(S) - \epsilon_F]/T}}, \quad (26)$$

and the correction $\delta\mathcal{F}$ is sought to linear order in \mathbf{E} . For the collision term we adopt the simplest approximation with relaxation time τ , so the linearized kinetic equation for $\delta\mathcal{F}$ has the form:

$$\frac{\partial \delta\mathcal{F}}{\partial t} + \omega_c(S) \frac{\partial \delta\mathcal{F}}{\partial \phi} + \frac{\partial \mathcal{F}_0}{\partial S} \sum_n em_c \mathbf{E} \cdot \mathbf{v}_n e^{-in\phi} = -\frac{\delta\mathcal{F}}{\tau}, \quad (27)$$

For the monochromatic field, Eq. (14), one readily finds the oscillating correction $\delta\mathcal{F}(t) = \delta\mathcal{F}_\omega e^{-i\omega t} + \delta\mathcal{F}_\omega^* e^{i\omega t}$, with $\delta\mathcal{F}_\omega$ given by

$$\delta\mathcal{F}_\omega = -\frac{\partial \mathcal{F}_0}{\partial S} \sum_{n=-\infty}^{\infty} \frac{em_c \mathbf{v}_n \cdot \mathbf{E}_\omega}{1/\tau - i(\omega + n\omega_c)} e^{-in\phi}. \quad (28)$$

Substituting this expression in Eq. (24) and passing from integration over S to integration over ϵ , we obtain the current, $\mathbf{j}(t) = \mathbf{j}_\omega e^{-i\omega t} + \mathbf{j}_\omega^* e^{i\omega t}$, with \mathbf{j}_ω given by

$$\mathbf{j}_\omega = \frac{e^2}{2\pi\hbar^2} \int d\epsilon \left(-\frac{\partial f}{\partial \epsilon} \right) \sum_{n=-\infty}^{\infty} \frac{m_c \mathbf{v}_n (\mathbf{v}_n^* \cdot \mathbf{E}_\omega)}{1/\tau - i(\omega - n\omega_c)}. \quad (29)$$

Up to now we considered the problem at fixed k_z (recall that $m_c, \omega_c, \mathbf{v}_n$ depend on k_z via $\cos k_z a_z$). The obtained current should be summed over k_z with the help of

$$\sum_{k_z} \rightarrow \int_{-\pi/(2a_z)}^{\pi/(2a_z)} \frac{N_z a_z dk_z}{2\pi}, \quad (30)$$

where N_z is the number of graphene layers, and thus $N_z a_z$ is the thickness of the sample. Also, the result should be multiplied by the spin multiplicity 2, and by the valley multiplicity $\mathcal{N} = 2$. This gives the in-plane conductivity per graphene layer, which should be further divided by a_z to obtain the bulk conductivity,

$$\begin{aligned} \sigma_{ij}(\omega) &= \frac{2\mathcal{N}e^2}{2\pi\hbar^2 a_z} \int d\epsilon \left(-\frac{\partial f}{\partial \epsilon} \right) \int_{\pi/2}^{\pi/2} \frac{d(k_z a_z)}{2\pi} \times \\ &\times \sum_{n=-\infty}^{\infty} \frac{m_c v_{i,n} (v_{j,n})^*}{\Gamma - i(\omega - n\omega_c)}, \end{aligned} \quad (31)$$

where $\Gamma = 1/\tau$. The $B \rightarrow 0$ limit is recovered by setting $\omega_c \rightarrow 0$ and

$$\sum_{n=-\infty}^{\infty} v_{i,n} v_{j,n}^* \rightarrow \langle v_i v_j \rangle_\epsilon \equiv \frac{\int v_i v_j \delta(\epsilon_{k_z}(\mathbf{p}) - \epsilon) dp_x dp_y}{\int \delta(\epsilon_{k_z}(\mathbf{p}) - \epsilon) dp_x dp_y}. \quad (32)$$

We evaluate this integral numerically, and plot the corresponding dc conductivity in zero magnetic field in Fig. 5.

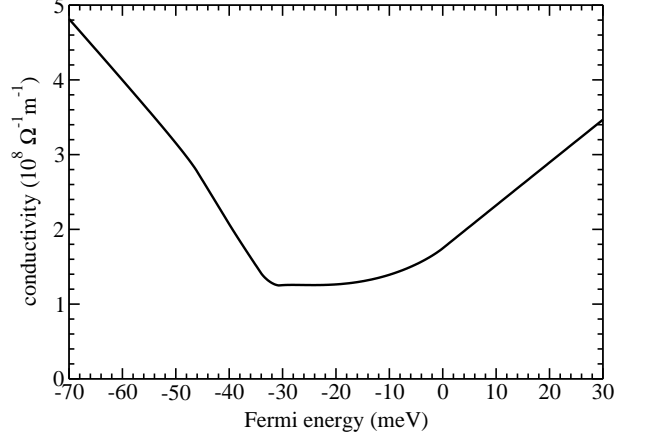


FIG. 5. The in-plane dc conductivity of graphite at zero temperature and zero magnetic field for $\hbar/\tau = 40 \mu\text{eV}$, as a function of the Fermi energy.

SELF-CONSISTENT BORN APPROXIMATION IN HIGH MAGNETIC FIELDS FOR ARBITRARY ELECTRONIC DISPERSION

Here we show that the self-consistent Born approximation, studied in detail for two-dimensional electron gas with parabolic dispersion by Ando and Uemura[2, 3], can be straightforwardly generalized to arbitrary electronic dispersion for short-range disorder and strong magnetic field. Moreover, the expressions obtained by Ando and Uemura for the broadening of the Landau levels and the cyclotron resonance lines remain unchanged.

Consider two-dimensional electrons with a dispersion law $\epsilon(\mathbf{p})$. The uniform magnetic field \mathbf{B} is perpendicular to the plane, and is described by the vector potential \mathbf{A} . In the presence of a static disordered potential $V(\mathbf{r})$, the electronic Hamiltonian takes the form

$$\hat{H} = \epsilon(-i\hbar\nabla - e\mathbf{A}/c) + V(\mathbf{r}) \equiv \hat{H}_0 + \hat{H}_{dis}. \quad (33)$$

The random potential is assumed to be Gaussian with zero average, $\overline{V(\mathbf{r})} = 0$, and is determined by its pair correlator,

$$\overline{V(\mathbf{r})V(\mathbf{r}')} = W(\mathbf{r} - \mathbf{r}') = W_0 \delta(\mathbf{r} - \mathbf{r}'), \quad (34)$$

where the overbar denotes the average over the disorder realizations. If the disorder is due to random impurities with the two-dimensional density n_{imp} , and each impurity has a short-range potential $u_{\text{imp}}(\mathbf{r})$, then

$$W_0 = n_{\text{imp}} \left| \int u_{\text{imp}}(\mathbf{r}) d^2\mathbf{r} \right|^2. \quad (35)$$

Let us define the disorder-free Green's function:

$$\begin{aligned} G_0(\mathbf{r}, \mathbf{r}'; \epsilon) &= \langle \mathbf{r} | (\epsilon - \hat{H}_0)^{-1} | \mathbf{r}' \rangle = \\ &= \sum_{l,\alpha} \frac{\psi_{l\alpha}(\mathbf{r}) \psi_{l\alpha}^*(\mathbf{r}')}{\epsilon - \epsilon_l} \equiv \sum_l \frac{\mathcal{P}_l(\mathbf{r}, \mathbf{r}')}{\epsilon - \epsilon_l}. \end{aligned} \quad (36)$$

Here l labels the Landau levels with energies ϵ_l , and α labels states on the same Landau level with wave functions $\psi_{l\alpha}(\mathbf{r})$ (eigenfunctions of \hat{H}_0). For example, in the Landau gauge, $A_x = -By$, they can be labeled by the momentum p_x :

$$\psi_{lp_x}(x, y) = e^{ip_x/\hbar} \chi_l(y + cp_x/eB), \quad (37a)$$

where the functions $\chi_l(y)$ and Landau level energies ϵ_l are found from the following equation:

$$\epsilon(eBy/c, -i\hbar\partial_y) \chi_l(y) = \epsilon_l \chi_l(y). \quad (37b)$$

The choice of basis in the degenerate manifold of each Landau level, as well as the specific form of the wave functions will not be important. We will only need the following general properties: (i) the projector kernel $\mathcal{P}_l(\mathbf{r}, \mathbf{r}')$ depends only on the relative coordinate $\mathbf{r} - \mathbf{r}'$ (and so does the Green's function G_0), and (ii) the degeneracy of each Landau level is $L_x L_y / (2\pi\ell_B^2)$, where L_x and L_y are the dimensions of the sample in the x and y directions, respectively, and $\ell_B^2 = \hbar c / (eB)$. Thus,

$$\mathcal{P}_l(\mathbf{r}, \mathbf{r}') = \frac{1}{2\pi\ell_B^2}. \quad (38)$$

In the presence of disorder, one can define the full Green's function for each disorder realization,

$$G(\mathbf{r}, \mathbf{r}'; \epsilon) = \langle \mathbf{r} | (\epsilon - \hat{H})^{-1} | \mathbf{r}' \rangle = \sum_s \frac{\phi_s(\mathbf{r}) \phi_s^*(\mathbf{r}')}{\epsilon - E_s}, \quad (39)$$

(ϕ_s and E_s being the wave functions and energies of the exact eigenstates of \hat{H}), as well as its average over the realization, $\overline{G(\mathbf{r}, \mathbf{r}'; \epsilon)}$, from which several physical quantities may be obtained, as will be seen below. In the so-called self-consistent Born approximation (SCBA), which can be represented diagrammatically using the standard rules[4] as shown in Fig. 6(b), one obtains the following system of closed equations for the average Green's function \overline{G} and the self-energy Σ [4]:

$$\overline{G(\mathbf{r}, \mathbf{r}')} = G_0(\mathbf{r}, \mathbf{r}') + \int G_0(\mathbf{r}, \mathbf{r}_1) \Sigma(\mathbf{r}_1, \mathbf{r}_2) \overline{G(\mathbf{r}_2, \mathbf{r}')} d\mathbf{r}_1 d\mathbf{r}_2, \quad (40a)$$

$$\Sigma(\mathbf{r}, \mathbf{r}') = W(\mathbf{r} - \mathbf{r}') \overline{G(\mathbf{r}, \mathbf{r}')}. \quad (40b)$$

The ϵ argument, common for all functions, has been omitted for the sake of compactness. SCBA in strong magnetic fields has been analyzed in Ref. 2 for the parabolic dispersion, $\epsilon(\mathbf{p}) = p^2/(2m)$, and was shown to be valid for high Landau levels[5], in agreement with the general rule[4]: SCBA is valid when the electron motion between successive scattering events is quasiclassical (i. e., contains many de Broglie wavelengths). Even when this condition is fulfilled, the SCBA misses effects related to coherent multiple-impurity scattering, but such effects are beyond the scope of the present work.

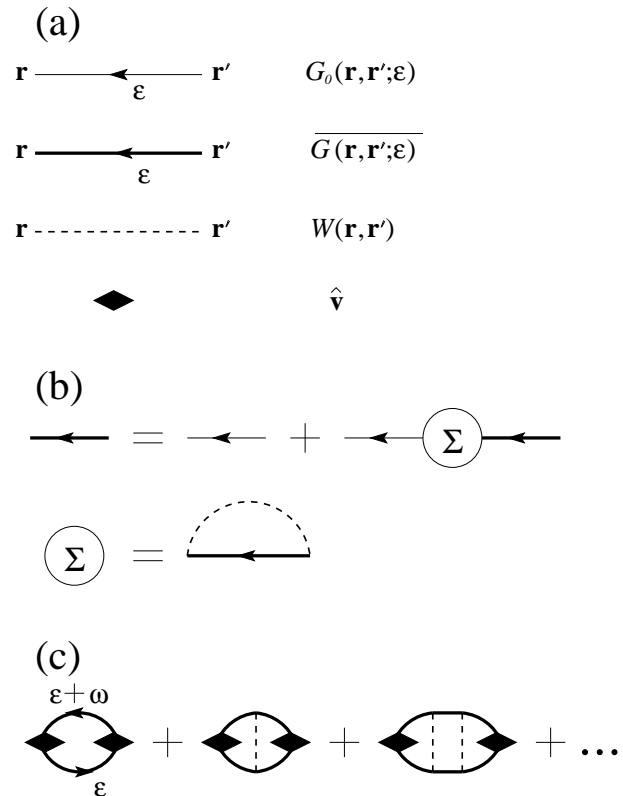


FIG. 6. (a) Notations for different elements, constituting the diagrams. (b) diagrammatic representation of the SCBA equations (40a), (40b). (c) SCBA diagrams for the disorder-averaged conductivity. SCBA, sometimes also called the non-crossing approximation, corresponds to neglecting all diagrams with crossing dashed lines.

Below we show that for the δ -correlated disorder, Eq. (34), and for strong magnetic fields, the SCBA equations (40a), (40b) are straightforwardly solved for any dispersion law $\epsilon(\mathbf{p})$. Indeed, since $W(\mathbf{r} - \mathbf{r}') = W_0 \delta(\mathbf{r} - \mathbf{r}')$, and since $\overline{G(\mathbf{r}, \mathbf{r}'; \epsilon)}$ does not depend on \mathbf{r} , Eq. (40b) gives $\Sigma(\mathbf{r}, \mathbf{r}'; \epsilon) = \Sigma(\epsilon) \delta(\mathbf{r} - \mathbf{r}')$. Thus, $\Sigma(\mathbf{r}, \mathbf{r}'; \epsilon)$ has no matrix elements between different Landau levels, so

$$\overline{G(\mathbf{r}, \mathbf{r}'; \epsilon)} = \sum_l \frac{\mathcal{P}_l(\mathbf{r}, \mathbf{r}')}{\epsilon - \epsilon_l - \Sigma(\epsilon)}. \quad (41)$$

For $\Sigma(\epsilon)$ we have the self-consistency equation, which can be written as

$$\Sigma(\epsilon) = \sum_l \frac{\gamma_B^2}{\epsilon - \epsilon_l - \Sigma(\epsilon)}, \quad \gamma_B^2 = \frac{W_0}{2\pi\ell_B^2} \quad (42)$$

where we used Eq. (38). It is convenient to express the factor γ_B^2 in terms of the cyclotron frequency $\omega_c = (\epsilon_{l+1} - \epsilon_l)/\hbar$ and the zero-field scattering rate $1/\tau_{B=0}$, assuming that both vary weakly with energy on the scale of $\hbar\omega_c$. The self-consistent Born approximation at zero

field gives [4]

$$\frac{\hbar}{\tau_{B=0}} = 2\pi\mathcal{N}W_0\nu, \quad (43)$$

where \mathcal{N} is the number of valleys (provided that the disorder is sufficiently short-range to induce efficient intervalley scattering), and ν is the density of states per unit area per spin projection and per valley at zero field. When the energy dependence of ν is weak, one can write

$$\nu \approx \frac{1}{\hbar\omega_c} \frac{1}{2\pi\ell_B^2}, \quad (44)$$

since each Landau level has $1/(2\pi\ell_B^2)$ states per unit area, and $\hbar\omega_c$ is the separation between the Landau levels. This gives

$$\gamma_B^2 = \frac{\hbar}{\tau_{B=0}} \frac{\hbar\omega_c}{2\pi\mathcal{N}}. \quad (45)$$

In the limit of strong fields, $\omega_c\tau_{B=0} \gg 1$, we have $\gamma_B \ll \epsilon_l - \epsilon_{l'}$. Let us focus on some Landau level l and on energies E close to ϵ_l . First, let us consider terms in the sum in Eq. (42) corresponding to levels different from the chosen level l . They result in a small overall shift of the level l :

$$\tilde{\epsilon}_l \approx \epsilon_l + \Sigma(\epsilon_l) \approx \epsilon_l + \sum_{l' \neq l} \frac{\gamma_B^2}{\epsilon_l - \epsilon_{l'}}. \quad (46)$$

In the following we will neglect the difference $\tilde{\epsilon}_l - \epsilon_l \sim \gamma_B^2/(\hbar\omega_c)$, which is much smaller than the Landau level broadening, as we will see shortly. The term in the sum in Eq. (42), corresponding to the same level l , should be treated exactly; it results in a quadratic equation for $\Sigma(\epsilon)$. As a result, we can write

$$\Sigma(\epsilon) = \frac{\epsilon - \epsilon_l}{2} - \sqrt{\frac{(\epsilon - \epsilon_l)^2}{4} - \gamma_B^2} + \sum_{l' \neq l} \frac{\gamma_B^2}{\epsilon - \epsilon_{l'}}, \quad (47)$$

for $|\epsilon - \epsilon_l| \ll \hbar\omega_c$.

The knowledge of $\Sigma(\epsilon)$, Eq. (47), and of $\overline{G(\mathbf{r}, \mathbf{r}'; \epsilon)}$, Eq. (41), enables us to find the disorder-averaged density of states per unit area per spin projection and per valley:

$$\overline{\nu(\epsilon)} = \frac{1}{\pi} \text{Im} \overline{G(\mathbf{r}, \mathbf{r}; \epsilon - i0^+)} = \sum_l \frac{\rho(\epsilon - \epsilon_l)}{2\pi\ell_B^2}, \quad (48a)$$

$$\rho(\epsilon) = \frac{1}{\pi\gamma_B} \sqrt{1 - \left(\frac{\epsilon}{2\gamma_B}\right)^2}. \quad (48b)$$

Thus, each Landau level, which in the absence of disorder is discrete and infinitely degenerate, in the presence of disorder is broadened into a semicircle.

To describe the cyclotron resonance (that is, inter-Landau-level absorption), we start from the expression for two-dimensional conductivity in terms of the exact

wave functions $\phi_s(\mathbf{r})$ and energies E_s , following directly from the Kubo formula:

$$\begin{aligned} \sigma_{ij}^{(2)}(\omega) &= \frac{2\mathcal{N}ie^2}{\omega L_x L_y} \sum_s f_s \langle s | \hat{m}_{ij}^{-1} | s \rangle + \\ &+ \frac{2\mathcal{N}ie^2}{\omega L_x L_y} \sum_{ss'} \frac{(f_s - f_{s'}) \langle s | \hat{v}_i | s' \rangle \langle s' | \hat{v}_j | s \rangle}{\hbar\omega - (E_{s'} - E_s) + i0^+} \\ &= \frac{2\mathcal{N}i\hbar e^2}{L_x L_y} \sum_{ss'} \frac{(f_s - f_{s'}) \langle s | \hat{v}_i | s' \rangle \langle s' | \hat{v}_j | s \rangle}{(E_{s'} - E_s)(\hbar\omega - E_{s'} + E_s + i0^+)}. \end{aligned} \quad (49)$$

Here we used the notations

$$\hat{\mathbf{v}} = \frac{\partial \epsilon(\mathbf{p})}{\partial \mathbf{p}} \Big|_{\mathbf{p} \rightarrow -i\hbar\nabla}, \quad \hat{m}_{ij}^{-1} = \frac{\partial^2 \epsilon(\mathbf{p})}{\partial p_i \partial p_j} \Big|_{\mathbf{p} \rightarrow -i\hbar\nabla}, \quad (50)$$

and the last equality in Eq. (49) was obtained using the commutation relations

$$\hat{m}_{ij}^{-1} = \frac{i}{\hbar} [\hat{v}_i, x_j], \quad \hat{\mathbf{v}} = \frac{i}{\hbar} [\hat{H}_0, x_j]. \quad (51)$$

Introducing the notation

$$G^{R-A}(\mathbf{r}, \mathbf{r}'; \epsilon) = G(\mathbf{r}, \mathbf{r}'; \epsilon + i0^+) - G(\mathbf{r}, \mathbf{r}'; \epsilon - i0^+), \quad (52)$$

we can write the dissipative part of the conductivity, averaged over the disorder, as

$$\begin{aligned} \overline{\text{Re} \sigma_{xx}^{(2)}(\omega)} &= \frac{2\mathcal{N}e^2}{4\pi\omega} \int d\epsilon [f(\epsilon + \hbar\omega) - f(\epsilon)] \int \frac{d^2\mathbf{r} d^2\mathbf{r}'}{L_x L_y} \\ &\times \overline{\hat{v}_x G^{R-A}(\mathbf{r}, \mathbf{r}'; \epsilon + \hbar\omega) \hat{v}_x' G^{R-A}(\mathbf{r}', \mathbf{r}; \epsilon)}. \end{aligned} \quad (53)$$

This expression involves the average of products of two Green's functions, which in SCBA reduces to summation of the ladder series, shown in Fig. 6(c). Consider the second term in this series, containing one impurity line. It contains the spatial integral

$$\int d^2\mathbf{r}_1 W_0 J_{\epsilon, \epsilon \pm \hbar\omega}^{\pm, \pm}(\mathbf{r}_1) J_{\epsilon \pm \hbar\omega, \epsilon}^{\pm, \pm}(\mathbf{r}_1),$$

where \mathbf{r}_1 is the position of the impurity and

$$J_{\epsilon, \epsilon'}^{\pm, \pm}(\mathbf{r}_1) = \int d^2\mathbf{r} \overline{G(\mathbf{r}_1, \mathbf{r}; \epsilon \pm i0^+)} \hat{v}_x \overline{G(\mathbf{r}, \mathbf{r}_1; \epsilon \pm i0^+)}. \quad (54)$$

Since the average Green's functions depend only on the relative coordinate, $J_{\epsilon, \epsilon'}^{\pm, \pm}(\mathbf{r}_1)$ does not depend on \mathbf{r}_1 , and thus it can be written as

$$J_{\epsilon, \epsilon'}^{\pm, \pm} = \int \frac{d^2\mathbf{r} d^2\mathbf{r}_1}{L_x L_y} \overline{G(\mathbf{r}_1, \mathbf{r}; \epsilon \pm i0^+)} \hat{v}_x \overline{G(\mathbf{r}, \mathbf{r}_1; \epsilon \pm i0^+)}. \quad (55)$$

Recalling Eq. (41) for the Green's function, we note that because of the integration over \mathbf{r}_1 , the contribution to transitions between different Landau levels l and l' involves the product of the projectors $\hat{\mathcal{P}}_l \hat{\mathcal{P}}_{l'} = 0$. Thus,

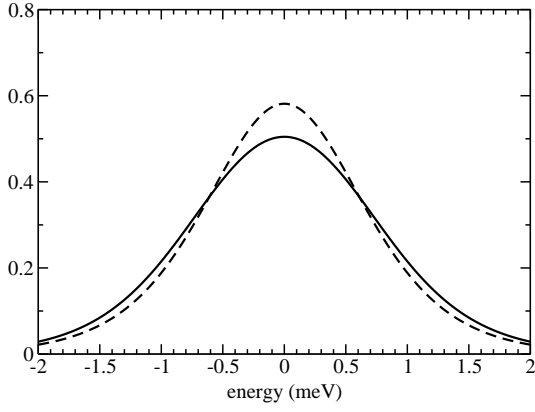


FIG. 7. Plot of $[f(\epsilon - \hbar\omega) - f(\epsilon + \hbar\omega)]/(\hbar\omega)$ (solid line) and $-\partial f(\epsilon)/\partial\epsilon$ (dashed line) as a function of $\epsilon - \epsilon_F$ for $T = 0.43$ meV, $\hbar\omega = 1.17$ meV.

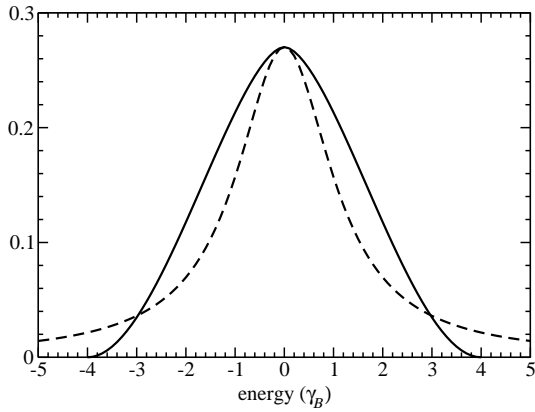


FIG. 8. Plot of the convolution $\int \rho(\epsilon - \hbar\tilde{\omega}/2) \rho(\epsilon + \hbar\tilde{\omega}/2) d\epsilon$ (solid line) and of the Lorentzian profile $(\Gamma/\pi\hbar)/(\tilde{\omega}^2 + \Gamma^2)$ (dashed line) as a function of $\hbar\tilde{\omega}/\gamma_B$ for $\Gamma = (3\pi/8)(\gamma_B/\hbar)$.

only the first term of the ladder series in Fig. 6(c) contributes to the inter-Landau-level transition, in full analogy with the case of the parabolic spectrum[3].

Explicitly, from Eq. (41) we obtain

$$\begin{aligned} \overline{\text{Re } \sigma_{xx}^{(2)}(\omega)} &= 2\mathcal{N}\pi e^2 \int d\epsilon \frac{f(\epsilon - \hbar\omega/2) - f(\epsilon + \hbar\omega/2)}{\hbar\omega} \\ &\times \sum_{l,l'} \hbar \rho(\epsilon - \hbar\omega/2 - \epsilon_l) \rho(\epsilon + \hbar\omega/2 - \epsilon_{l'}) \\ &\times \sum_{\alpha,\alpha'} |\langle l, \alpha | \hat{v}_x | l', \alpha' \rangle|^2. \end{aligned} \quad (56)$$

In this expression the disorder enters only in the densities of states, $\rho(\epsilon)$, while the velocity matrix elements are the same as in the absence of disorder. Moreover, when the quasiclassical approximation is valid, (ϵ_l depends smoothly on l) they can be calculated classically. Indeed, comparing Eqs. (31) and (56), one can establish the correspondence

$$-\frac{\partial f}{\partial\epsilon} \leftrightarrow \frac{f(\epsilon - \hbar\omega/2) - f(\epsilon + \hbar\omega/2)}{\hbar\omega}, \quad (57a)$$

$$|v_{x,n}|^2 \leftrightarrow \frac{2\pi\ell_B^2}{L_x L_y} \sum_{\alpha,\alpha'} |\langle l, \alpha | \hat{v}_x | l+n, \alpha' \rangle|^2, \quad (57b)$$

$$\frac{\Gamma/\pi}{\tilde{\omega}^2 + \Gamma^2} \leftrightarrow \hbar \int \rho(\epsilon) \rho(\epsilon + \hbar\tilde{\omega}) d\epsilon, \quad (57c)$$

where we denoted $\tilde{\omega} = \omega - n\omega_c$ or $\omega - (\epsilon_{l+n} - \epsilon_l)/\hbar$. The first two lines hold reasonably well in our case (even though $T = 5$ K = 0.43 meV < $\hbar\omega = 1.17$ meV, see Fig. 7), while in the third one the convolution of two semicircles is somewhat different from a Lorentzian, so there is no unique relation between Γ and γ_B . We choose to match the peak heights (that is, the value at $\tilde{\omega} = 0$), which fixes

$$\Gamma = \frac{3\pi}{8} \frac{\gamma_B}{\hbar}, \quad (58)$$

as illustrated by Fig. 8.

-
- [1] A. A. Abrikosov, *Fundamentals of the Theory of Metals* (North Holland, Amsterdam, 1988).
 - [2] T. Ando and Y. Uemura, J. Phys. Soc. Japan **36**, 959 (1974).
 - [3] T. Ando, J. Phys. Soc. Japan **38**, 989 (1975).
 - [4] A. A. Abrikosov, L. P. Gorkov, and I. E. Dzyaloshinski, *Methods of Quantum Field Theory in Statistical Physics* (Dover, New York, 1963).
 - [5] T. Ando, J. Phys. Soc. Japan **37**, 622 (1974).